RESEARCH ARTICLE | MARCH 24 2025

Backward wave optical parametric oscillator pumped by subnanosecond microlaser pulses

J. Banys ; J. Jakutis Neto ; A. Žukauskas ; V. Pašiškevičius ; V. Jarutis ; J. Vengelis

APL Photonics 10, 036123 (2025)
https://doi.org/10.1063/5.0256256

APL Photonics ARTICLE pubs.aip.org/aip/app

Backward wave optical parametric oscillator pumped by subnanosecond microlaser pulses

Cite as: APL Photon. 10, 036123 (2025); doi: 10.1063/5.0256256
Submitted: 3 January 2025 • Accepted: 28 February 2025 •
Published Online: 24 March 2025

J. Banys,[1,a)] J. Jakutis Neto,[1,2] A. Žukauskas,[3] V. Pašiškevičius,[3] V. Jarutis,[1] and J. Vengelis[1]

AFFILIATIONS

[1] Laser Research Center, Faculty of Physics, Vilnius University, Saulėtekio ave. 10, 10223 Vilnius, Lithuania
[2] Department of Aerospace Science and Technology, Institute for Advanced Studies (IEAv), Trevo Cel. Av. José A. A. do Amarante, 01, São José dos Campos-SP 12228-001, Brazil
[3] Department of Applied Physics, Royal Institute of Technology (KTH), Roslagstullsbacken 21, Stockholm 10691, Sweden

[a)] Author to whom correspondence should be addressed: jonas.banys@ff.vu.lt

ABSTRACT

Microlaser-pumped subnanosecond pulse duration optical parametric generators have great potential to establish themselves as a compact, simple, and cost-effective option for various tasks that do not require high temporal resolution. However, fundamental limitations of co-propagating three-wave interaction, including broad bandwidth, non-transform-limited pulses, and suboptimal spatial coherence of the output, restrict their suitability for demands of high spectral purity and beam quality. In this report, we address these shortcomings and present the first Backward Wave Optical Parametric Oscillator (BWOPO) pumped by transform-limited subnanosecond pulses from Nd:YAG microlaser. This paper reports a thorough performance investigation of BWOPO setups pumped by the first (1064 nm) and second (532 nm) harmonics of the microlaser. Based on a periodically poled Rb-doped $KTiOPO_4$ crystal with a 427 nm grating period, BWOPO achieved nearly transform-limited pulses and diffraction-limited beams of the signal and idler waves in the near and mid-infrared with 50% conversion efficiency. A degenerate BWOPO operation is also presented. 792.5 nm wavelength pumped, temperature-tuned degenerate BWOPO generated a narrowband counter-propagating signal and idler centered at 1585 nm. This experiment also revealed thermal instability of the ferroelectric domain structure, resulting in a twofold decrease of the crystal's effective nonlinearity.

I. INTRODUCTION

In the context of optical parametric generators (OPGs) and oscillators (OPOs), the subnanosecond pulse duration range (~300 ps–1 ns) stands out as both unique and highly promising. For a long time, generating subnanosecond pulses was confined to complex active mode-locking lasers; however, the progress of Q-switched microlaser technologies enabled the development of reliable, compact, and cost-effective microlasers (microchip lasers) delivering single longitudinal mode mJ-level energy subnanosecond pulses, which currently serve as an efficient pump source for parametric devices.[1–4] Such systems can be viewed as a simpler, more compact, and affordable alternative for sophisticated ultrashort pulse parametric systems, particularly when high temporal resolution is not required for the application.[5,6] Tunable wavelength laser radiation of subnanosecond duration is of interest in transient absorption spectroscopy,[7] laser-induced breakdown spectroscopy,[8] laser-induced fluorescence,[9] LIDAR,[10] THz generation,[11,12] nonlinear optics[13] applications, and more.

As of now, periodically poled nonlinear media-based parametric devices utilizing type-0 quasi-phase-matching (QPM) have emerged as the primary means for the generation of near-to-mid-infrared subnanosecond laser pulses. Microlaser-based OPGs and OPOs tunable from ~1.4 to ~4.5 μm with kHz repetition rates delivering tens and hundreds of μJ of output pulse energies present the advantages of a simple design, high conversion efficiency, and broad wavelength tunability and are currently undergoing development.[2,14–17] However, the conventional microlaser-pumped OPG and OPO configurations have several fundamental limitations. First, large parametric gain bandwidth results in a signal and idler length-normalized bandwidth of above 300 GHz · cm, leading to the output subnanosecond pulses that are very far from transform-limited (TL) as their time-bandwidth products (TBPs) are in the 10^1–10^3 range.[14,15] The TBP of such systems can be improved by injection seeding the OPG with a distributed feedback continuous wave diode laser seeder; however, this is usually limited to a narrow wavelength range and comes at the expense of the device's design simplicity and cost-effectiveness.[2,18,19] Second, the spatial coherence of conventional OPGs and OPOs is suboptimal as the M^2 values of the signal and idler range from ∼2 to 8, primarily due to the inherent cascaded parametric conversion processes in type-0 QPM devices.[14,17,20] Finally, when larger pump beams are used, non-collinear QPM leads to non-homogeneous signal and idler spectra across the beam diameter, further reducing spectral purity and beam quality of the OPG output.[20]

A unique alternative to the microlaser-pumped OPGs and OPOs is the backward wave optical parametric oscillator (BWOPO). Initially proposed by Harris in 1966[21] and experimentally realized by Canalias and Pašiškevičius in 2007,[22] a BWOPO is based on a three-wave second-order nonlinear interaction in a QPM nonlinear medium where the pump wave is down-converted into counter-propagating signal and idler waves. The oscillation in a BWOPO is ensured by a distributed nonlinear feedback mechanism due to the presence of two counter-propagating waves. This feedback is integral to the nonlinear process and alleviates the need for an optical cavity, making it a very simple, reliable, and alignment-free device.[22,23] Therefore, in the literature, BWOPOs are sometimes referred to as mirrorless OPOs (MOPOs).[22,24]

A BWOPO not only provides inherent spatial separation of the output but also offers unique spectral and coherence properties of the parametric waves that differ significantly from those of conventional parametric devices utilizing co-propagating interaction. The QPM condition for a backward propagating signal reads

$$\Delta\mathbf{k} = \mathbf{k}_p + \mathbf{k}_s - \mathbf{k}_i - \mathbf{k}_G, \tag{1}$$

where $\mathbf{k}_{p,s,i}$ are the pump, signal, and idler wave vectors, $\mathbf{k}_G = 2\pi m/\Lambda$ is the QPM grating vector, m is the order of interaction, and Λ is the grating period. In the counter-propagating interaction geometry, the inherent phase mismatch (without QPM) becomes very large; thus, to compensate for it, the grating period Λ for the first-order QPM interaction must be on a submicrometer scale. In contrast to OPOs and OPGs, such highly constrained wave vector mismatch provides significantly better control over the output spectra—the forward wave can be treated as a wavelength-shifted spectral replica of the pump and inherits its phase modulation, while the backward wave is naturally narrowband.[22,25,26] Therefore, if the BWOPO is pumped with a TL pump pulse (from a microlaser, for example), one should expect a TL signal and idler output pulses. Moreover, the optimal temporal overlap of the interacting waves throughout the few-cm-long BWOPO crystal is achieved with pump pulses on the order of hundreds of picoseconds; thus, in our case, subnanosecond pulses provide the optimal BWOPO pump pulse duration, ensuring that the oscillation threshold is reached within a build-up time shorter than the duration of the pump pulse (i.e., without its depletion), thereby enabling the potential for high conversion efficiency.[24–26] Combined with the suppression of the back-conversion process[27] and the spatial mode cleanup of output,[23] such exceptional features render BWOPOs as an excellent choice for Q-switched subnanosecond microlaser pumping. By utilizing these properties, microlaser-pumped BWOPOs should achieve narrowband operation with high spatial coherence in a simple single-pass optical device, effectively addressing the limitations mentioned earlier and increasing the appeal of microlaser-pumped parametric systems, especially for applications demanding high spectral purity, such as spectroscopy[28] and remote sensing.[29]

The progress of periodic poling by coercive field engineering[27,30,31] allowed the development of periodically poled potassium titanyl phosphate (PPKTP) crystals with submicrometer grating periods. This led to the demonstration of various BWOPOs using nanosecond[23,32,33] and broadband chirped Ti:sapphire laser pump sources.[22,25,27,34] In this work, we contribute to the field and demonstrate the first BWOPO pumped by high-energy TL subnanosecond pulses from a passively Q-switched Nd:YAG microlaser, achieving nearly TL pulses and nearly diffraction-limited beams of the signal and idler waves in near and mid-infrared—features that conventional OPG and OPO setups cannot achieve. We present a thorough performance investigation of Rb-doped KTP (Rb:PPKTP) crystal-based BWOPOs pumped by the first (1064 nm) and second (532 nm) harmonics of the microlaser. In addition, by pumping the BWOPO crystal at a wavelength of 792.5 nm and tuning the crystal temperature up to 350 °C, we realized a degenerate BWOPO generating a narrowband counter-propagating signal and idler centered at 1585 nm. This experiment revealed a detrimental effect of elevated temperature of submicrometer grating period Rb:PPKTP crystal—thermal instability of the ferroelectric domain structure, confirmed by a twofold decrease of the crystal's effective nonlinearity.

II. OPTICAL EXPERIMENTS AND DISCUSSION

A. Subnanosecond BWOPO pumped by the first harmonic of the microlaser

The principal experimental setup of microlaser-pumped BWOPO is shown in Fig. 1. The pump source was a passively Q-switched Nd:YAG master oscillator power amplifier (MOPA) microlaser (Standa Ltd.) that generated 1064 nm wavelength TL subnanosecond (520 ps at FWHM) pulses at 1 kHz repetition rate with pulse energy up to 1 mJ and a nearly diffraction-limited beam quality. The pump was focused with a 250 mm focal length lens to a waist diameter of 200 μm ($1/e^2$ level). BWOPO gain media was a 1 mm thick, 6 mm wide, and 2 cm long Rb:PPKTP crystal. The QPM structure, featuring a single grating period of Λ = 427 nm, was created through coercive-field engineering and periodic poling. The facets of the crystal were left uncoated. For the temperature tuning, the crystal was placed into an oven that could be heated up to 200 °C using a temperature controller (HC Photonics) with a stability of 0.1 °C. The oven and the crystal were mounted on a three-axis translation stage with additional tilt and rotation adjustments. In this setup, the BWOPO generated an idler wave at 3303.5 nm co-propagating with the pump and a backward-propagating signal at 1569.5 nm. The signal and pump waves were separated by dichroic mirror DM1 (R > 99.5% at 1400–2128 nm, T ≈ 96% at 1064 nm). A filter removed parasitic reflections from DM1 and transmitted only the signal wave. The forward idler was collimated with a lens and separated from the pump with another dichroic mirror DM2

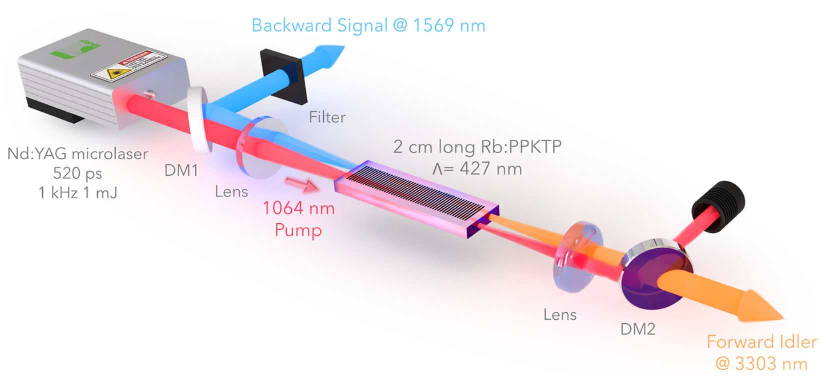

FIG. 1. Principal experimental setup of Rb:PPKTP-based BWOPO utilized transform-limited subnanosecond microlaser pulses as a pump source for the first time.

(R > 99% at 1064 nm, $T \approx$ 96% at 3303 nm). BWOPO output spectrum was measured using the ANDO AQ6317C (Yokogawa) optical spectrum analyzer (OSA) with a resolution of up to 10 pm. The input and output energy were measured using a thermopile-based power meter (3A, Ophir Optronics), and losses caused by Fresnel reflections from the uncoated crystal were accounted for. The spatial characteristics of the pump, signal, and idler beams were measured using Si-based Spiricon SP620U (Ophir Optronics) and InGaAs-based C12741-03 (Hamamatsu) cameras.

Our initial objective was to determine whether the microlaser-pumped BWOPO output exhibits a narrowband nature. Figure 2 presents the BWOPO backward signal spectra centered at 1569.52 nm measured using an optical spectrum analyzer. Since the Rb:PPKTP crystal was driven by the TL pump pulses, the BWOPO output achieved narrowband operation as the signal FWHM bandwidth was 28 pm. By measuring interference fringe visibility vs optical path length with a Michelson interferometer, we evaluated the coherence length l_c of the signal pulses. Given that $\Delta\lambda_s = \lambda_s^2/l_c$, the signal bandwidth was estimated to be around 22 pm (Fig. 2 dashed line), which coincided well with the OSA measurement. The idler was at 3303.5 nm and had an estimated bandwidth of 70 pm from the l_c measurement. Therefore, both counter-propagating parametric waves were naturally narrowband, with bandwidths up to three orders of magnitude smaller than those achieved with microlaser-based OPG and OPO setups.

We performed temporal characterization of the output pulses from the BWOPO using an autocorrelator. Autocorrelation traces (Fig. 3) yielded 320 and 295 ps pulses for the signal and idler, assuming a Gaussian pulse shape. This resulted in a signal TBP of 0.85 and an idler TBP of 0.57. Therefore, subnanosecond microlaser-pumped BWOPO allows us to obtain nearly TL signals and idler pulses from a simple OPG-like optical configuration—a result that would otherwise be attainable with conventional OPGs and OPOs relying on co-propagating interaction.

For microlaser-pumped parametric devices, it is important to determine whether the output spectral envelope remains uniform across the beam. For OPGs pumped by larger (>250 μm waist diameter) beams, non-collinear QPM will be observed, resulting in a conical, angularly chirped OPG output beam that exhibits large divergence and a broadband spectrum, thereby reducing both the spectral purity and the beam quality of the output.[20] We have measured the spectrum of the BWOPO signal as a function of the scanning position for two pump beam waist diameters d_p (Fig. 4). When d_p was 200 μm, the BWOPO signal spectrum was monotonous across its beam [Fig. 4(a)]. At d_p = 400 μm, the signal spectrum remained monotonous; however, in this case, the pump volume was sufficiently large to allow non-collinear QPM, which in BWOPO results as a broadening of the parametric wave bandwidth

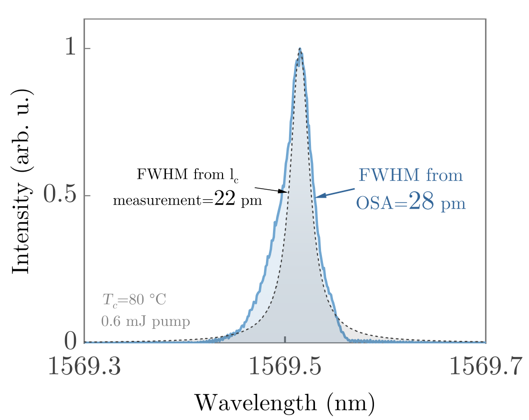

FIG. 2. Narrowband BWOPO backward signal spectra measured with an OSA (blue solid line) and calculated based on coherence length l_c measurements (black dashed line).

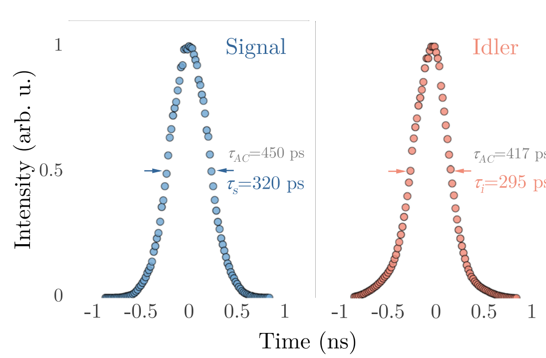

FIG. 3. Autocorrelation traces of the BWOPO backward signal and forward idler showed ~1.6–1.8 times shorter pulses compared to those of the pump.

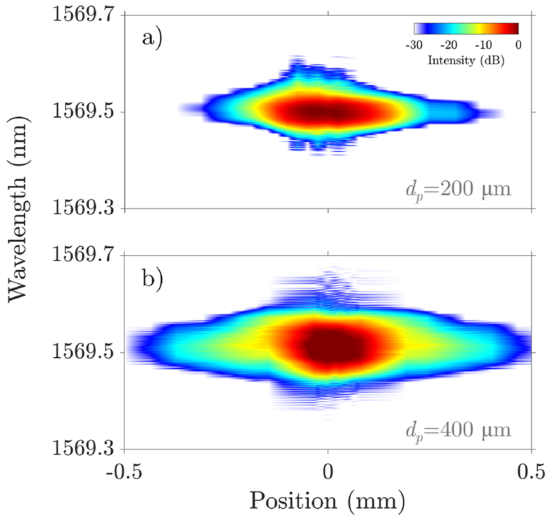

FIG. 4. Signal wave spectrum homogeneity measurements—spectra dependence on the scanning position for two pump beam waist diameters: 200 μm (a) and 400 μm (b).

[Fig. 4(b)].[33,38] Nevertheless, the backward signal still remained narrowband (58 pm FWHM).

Since the Rb:PPKTP crystal had a single grating period, wavelength tuning was restricted to adjusting the crystal temperature T_c. BWOPO signal and idler wavelength tuning with T_c is shown in Fig. 5. By changing the T_c from 24 to 200 °C, we achieved wavelength tuning of 4.64 nm for the signal and 20.45 nm for the idler, whereas the theoretical tuning curves from QPM conditions were only in partial agreement with experimental values. The calculated wavelength tuning rates were 0.0263 nm/°C for the signal and −0.116 nm/°C for the idler (or 3.2 GHz/K for both waves), which is more than ten times lower than those observed in the co-propagating interaction. Such temperature insensitivity is another distinctive BWOPO feature that can be seen ambiguously. On one hand, it ensures the device's high stability and precise wavelength tuning. On the other hand, for the applications of optical parametric devices requiring broader wavelength tunability, the implementation of multigrating or cascaded-multigrating submicrometer QPM structures would be necessary.

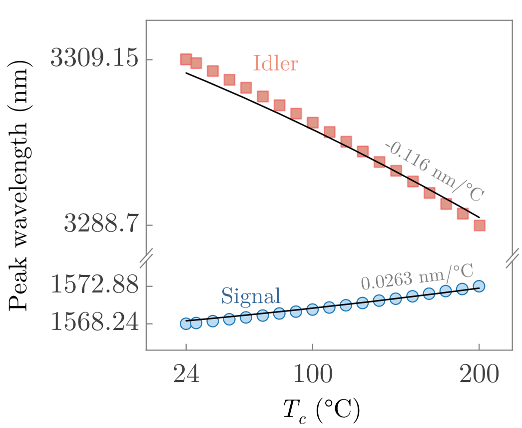

FIG. 5. BWOPO signal and idler wavelength temperature tuning rates were >10 times lower than for the co-propagating interaction. The idler wavelength was calculated using the energy conservation law. Black solid lines show calculated tuning curves from QPM conditions. Sellmeier's equation was taken from Katz,[35] thermo-optic coefficients from Emanueli,[36] and thermal expansion coefficients from Pignatiello.[37]

The BWOPO reached the oscillation threshold at 80 μJ of pump energy (Fig. 6). As the pump energy was further increased, linear growth of signal and idler energy was observed. At a maximum pump energy of 0.6 mJ (corresponding to a peak pump intensity of 6.8 GW/cm^2), 0.255 mJ of signal and 0.05 mJ of idler energy were obtained with slope efficiencies η_{slope} of 50% and 10%. The lower idler energies were due to partial absorption of the idler wavelength by the Rb:PPKTP crystal. The total BWOPO conversion efficiency reached 51%, a comparable result to conventional microlaser-based OPGs. What is unlike in OPGs and OPOs is that the BWOPO output vs pump energy dependence does not exhibit roll-off or saturation. The geometry of counter-propagating interaction results in a spatial separation of the signal and idler peak intensities, making back-conversion a very inefficient process in BWOPOs.[27] This should also prevent deterioration of the signal and idler beam quality as the pump energy is increased from threshold to maximum. Indeed, this was observed in our study: the BWOPO signal and idler beams remained very similar at near-threshold (0.1 mJ) and maximum (0.6 mJ) pump energies [Figs. 7(a) and 7(b)]. Using the knife edge method, we performed caustic measurements to determine the output beam quality parameter M^2. At 0.6 mJ pump energy, signal M^2 was 1.52 and 1.61, whereas the idler M^2 was 1.19 and 1.25 for the X and Y axes, respectively. Such a result is notably better compared to beam quality from conventional microlaser-pumped parametric devices, where M^2 values of the output are typically no less than 2.

Finally, we evaluated the periodic poling homogeneity of the 427 nm grating period Rb:PPKTP crystal. We used our nonlinear scanning technique, in which the aperture of the crystal was scanned in X and Y directions with very fine steps, and at each aperture point, the signal conversion efficiency η_{signal} was measured.[39] The

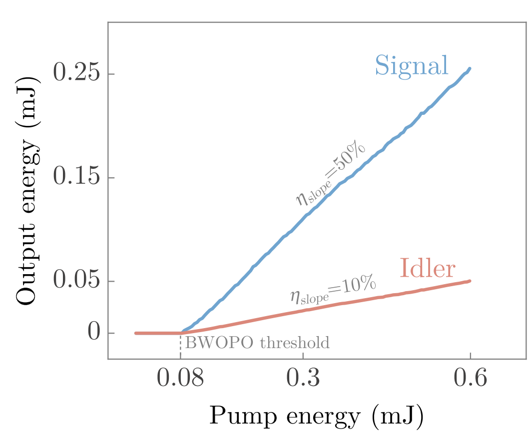

FIG. 6. Signal and idler energy grew linearly with increasing 1064 nm pump energy.

09 June 2025 07:20:48

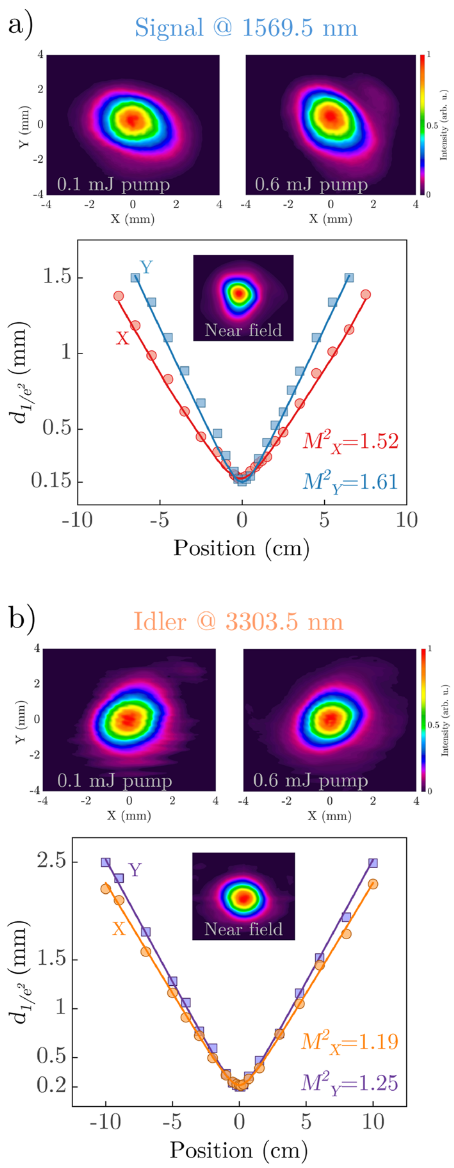

FIG. 7. BWOPO far-field signal and idler beam profiles exhibited similar patterns at both near-threshold and maximum pump energies. The M^2 measurements below indicated nearly diffraction-limited beam quality. Insets display the near-field beam profiles of the output.

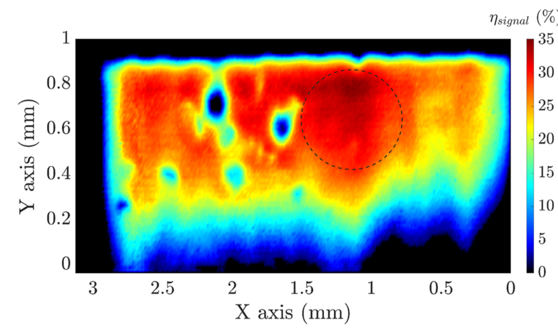

FIG. 8. Distribution of signal wave conversion efficiency, η_{signal}, varied with the transverse coordinates of the grating aperture. The region outlined by the dashed line denotes the most effective working zone of the crystal.

top part of the crystal generated with much higher conversion efficiency than the bottom (Fig. 8), suggesting a non-uniform domain duty cycle throughout the crystal thickness. The measurement also indicates that the submicrometer length ferroelectric domain ends in this crystal and are pinned down in the bulk, close to the polar surface opposite to the one that was initially patterned using UV-laser lithography. This might be relevant for the structure's stability at high temperatures. The conversion efficiency somewhat depended on the horizontal coordinate (X) as well. Low or zero-efficiency holes were most probably related not to the periodic poling but to the crystal surface defects. Nonetheless, bearing in mind the unique parameters of the periodically poled crystal (2 cm length QPM structure with Λ = 427 nm period) and the fact that the pump beam did not fully occupy the aperture of the crystal, such crystal poling quality homogeneity was sufficient. Therefore, for the whole study, we have confined the interaction to the crystal's most effective region, outlined by the dashed line in Fig. 8.

B. Subnanosecond BWOPO pumped by the second harmonic of the microlaser

An interesting feature of the counter-propagating parametric interaction is that the same period BWOPO crystal can be pumped by any wavelength as long as all interacting waves remain within the crystal's transparency range. This allowed us to evaluate the performance of a BWOPO pumped by the second harmonic (532 nm) of the same Nd:YAG microlaser. In this case, the BWOPO output switched directions and generated a backward idler at 1618.5 nm and a forward signal at 792.5 nm. The 450 ps (FWHM) duration 532 nm wavelength pump pulses were generated in a bulk KTP crystal; a dichroic mirror DM1 was changed to the one that reflects the pump and transmits the idler, and DM2 was replaced by a filter that transmits the signal and absorbs the residual pump. The pump was focused on a waist diameter of 250 μm (at $1/e^2$ level).

Narrowband BWOPO operation was achieved with 532 nm pumping as well [Fig. 9(a)]. The signal spectrum was calculated based on a coherence length l_c measurement, while the idler spectrum was measured with OSA. The forward signal, centered at 792.5 nm, exhibited a bandwidth of ~9 pm, whereas the backward idler at 1618.5 nm had a broader bandwidth of around 38 pm. Signal and idler pulses were roughly half the duration of the pump pulses, measuring about 220–230 ps using an autocorrelator [Figs. 9(b) and 9(c)]. This yielded TBPs of 0.94 and 1 for the signal and idler, respectively, indicating nearly TL output pulses, similar to the results obtained with the 1064 nm pump setup. 532 nm pumped BWOPO also had distinctively low wavelength temperature tuning rates of 0.04 nm/$^\circ$C for the idler and −0.0096 nm/$^\circ$C for the signal (or 4.6 GHz/K for both).

Compared to the 1064 nm pump configuration, the 532 nm pumped BWOPO had a five times lower oscillation threshold of 16 μJ (Fig. 10). As the pump was increased further, a linear rise

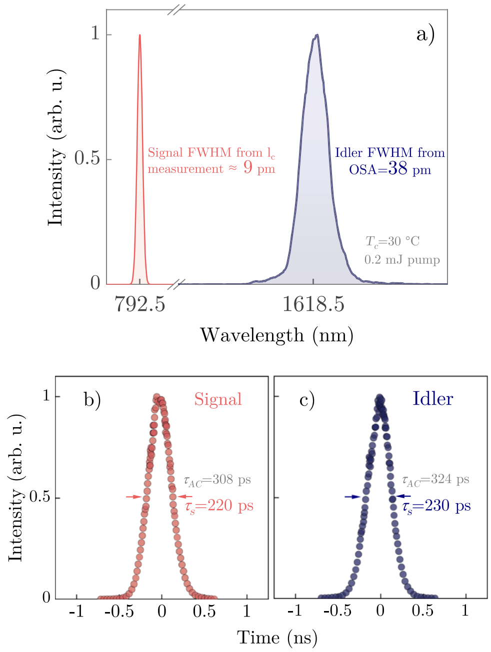

FIG. 9. Narrowband signal and idler spectra (a) with corresponding autocorrelation traces [(b) and (c)] of the 532 nm pumped BWOPO.

in output energy was observed with slope efficiencies of 42% for the signal and 18% for the idler. At a maximum 532 nm energy of 200 μJ, 74 μJ of signal, and 31 μJ of idler energy were obtained, achieving a combined conversion efficiency of 53%. The BWOPO output mode profiles were a bit poorer than in the 1064 nm pump case, as signal and idler beams had a broader low-intensity peripheral region (Fig. 10). Nevertheless, the BWOPO beam profiles and divergence were significantly better than those from second-harmonic microlaser-pumped OPGs.[14]

The BWOPO threshold can be used to estimate the effective second-order nonlinearity d_{eff} of the Rb:PPKTP crystal. Using the short-pulse Gaussian approximation from Godard *et al.*, the BWOPO threshold I_{th} is related to d_{eff} through the equation[26]

$$d_{\text{eff}} = \sqrt{\frac{4}{\pi \operatorname{erf}^2(1)}\left(1+\frac{\tau}{2\pi\tau_p}g_{\text{Log}}\right)^2 \frac{\varepsilon_0 c n_p n_s n_i \lambda_s \lambda_i}{32 L^2 I_{\text{th}}}}, \tag{2}$$

where τ is pump pulse propagation time through the crystal, τ_{p} is pump pulse duration, $g_{\text{Log}} = \ln(I_{\text{det}}/I_{\text{noise}})$ is proportional to the ratio of detectable intensity level I_{det} to the equivalent quantum noise intensity level I_{noise}, ε_0 is the permittivity of free space, c is the speed of light in vacuum, $n_{\text{p,s,i}}$ are the pump, signal, and idler refractive indices, $\lambda_{\text{s,i}}$ is the signal and idler wavelength, and L is the interaction length. In this case, I_{th} was 0.12 GW/cm^2, thus the estimated d_{eff} of the crystal was around 3.6 pm/V, which was approximately three times lower than for the ideal PPKTP type-0 QPM device (10.7 pm/V). The reduced nonlinearity was likely due to the suboptimal domain duty cycle of the 427 nm period QPM structure; however, it was still sufficient to achieve an efficient BWOPO process.

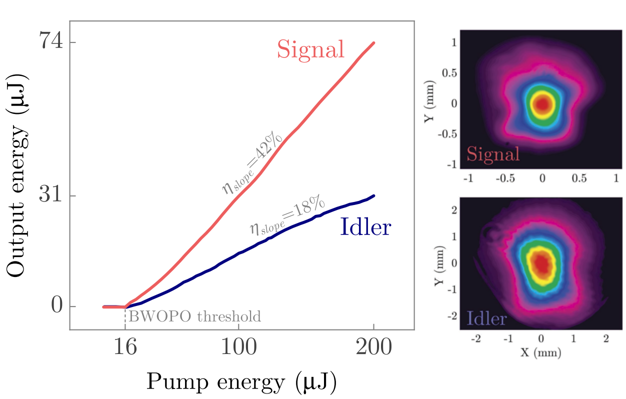

FIG. 10. 532 nm pumped BWOPO oscillation threshold was five times lower than that of the first harmonic pumped setup as shown in output energy vs pump energy dependence. Adjacent are the far-field beam profiles of the signal and idler.

C. Subnanosecond degenerate BWOPO

Given that the counter-propagating three-wave interaction imparts unique characteristics to the output radiation, it would also be interesting to investigate the performance of the BWOPO at the degenerate regime, where the signal and idler wavelengths coincide. Recently, the first degenerate BWOPO was demonstrated, which was pumped by chirped Ti:sapphire laser pulses and exhibited distinctive features like self-established phase-locking and both forward and backward sum-frequency generation.[34] Here, we show that it is also possible to achieve a degenerate BWOPO regime by tuning the temperature of the BWOPO crystal. The degenerate BWOPO was pumped by 792.5 nm wavelength narrowband subnanosecond pulses from another BWOPO that was based on the 1 cm long Rb:PPKTP crystal with the same 427 nm QPM grating period and pumped by the microlaser's second harmonic. The pump was focused with a 75 mm focal length lens into the degenerate BWOPO gain media, which was another 2 cm long Rb:PPKTP crystal with a QPM period of 427 nm. The crystal was placed in a homemade crystal oven capable of heating the sample up to 440 °C. A long-pass dichroic mirror (reflects the pump, transmits the backward wave) and a filter (blocks the pump and transmits the forward wave) were used to separate the interacting waves.

The 427 nm grating period was unsuitable for realizing degeneracy at near room temperature; therefore, to achieve it, the temperature of the Rb:PPKTP crystal had to be significantly increased. BWOPO wavelength temperature tuning calculations estimated that the degeneracy would be obtained at a crystal temperature of around 310 °C. Note that for crystals with submicrometer grating periods, it is important to include the thermal expansion of the crystal and its impact on the period when calculating temperature tuning curves.[32] Figure 11(a) shows BWOPO output spectra as a function of crystal temperature T_c, measured with OSA at 10 °C intervals. At T_c of 30 °C, the 792.5 nm pumped BWOPO generated a forward idler wave at 1595.81 nm and a backward signal at 1574.33 nm. As the T_c increased, the idler wavelength gradually decreased, whereas the signal wavelength increased up to the point of degeneracy, which was achieved at the T_c of 320 °C. At this temperature, the forward

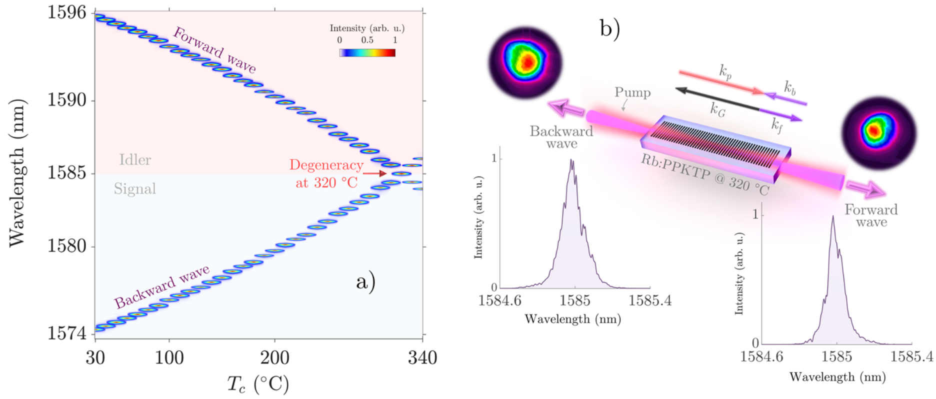

FIG. 11. As the crystal temperature (T_c) increased, the 792.5 nm pumped BWOPO signal and idler spectra converged up to the point of degeneracy at T_c = 320 °C (a). An illustration of a degenerate BWOPO concept, including the phase-matching diagram, output spectra, and far-field beam profiles (b).

and backward wave vectors canceled out, $\mathbf{k}_G$ fully compensated $\mathbf{k}_p$, and BWOPO generated a counter-propagating signal and idler centered at 1585 nm, as shown in the concept of a degenerate BWOPO in [Fig. 11(b)]. Due to the narrowband pump, the output spectra across the T_c range maintained a narrowband characteristic, with an average spectral FWHM of ~74 pm. This behavior contrasts with co-propagating microlaser-pumped parametric devices, where the spectral bandwidth at degeneracy significantly broadens, reaching hundreds of nm.[20] The output mode profiles at the degeneracy were also of decent quality [Fig. 11(b)].

Another distinctive feature of a BWOPO is its ability to achieve QPM even beyond the degeneracy point, a behavior not observed in co-propagating parametric devices. When the crystal was heated beyond T_c = 320 °C, parametric generation persisted; however, the wave directions reversed—the forward-propagating idler began traveling backward, while the backward-propagating signal moved forward [Fig. 11(a)]. During this experiment, we also observed that as the temperature of the crystal increased, the forward wave energy decreased (Fig. 12). At T_c = 30 °C, forward wave energy was 3.2 μJ, whereas at T_c = 320 °C it had reduced to 1.7 μJ. A more rapid decrease in energy was observed beyond 320 °C, and at 350 °C, the BWOPO ceased generating entirely. We have translated the crystal in the X and Y directions, but no generation was observed. Notably, the peak pump intensity of 792.5 nm pulses was low (<0.3 GW/cm^2); thus, laser-induced damage can be ruled out as a lack of generation cause. Afterward, the crystal was cooled to room temperature and pumped with 532 nm pulses with exactly the same experimental conditions described in Sec. II B. This was performed to assess the impact of annealing on the QPM structure by estimating the second-order nonlinearity (d_{eff}) of the Rb:PPKTP. The initial BWOPO threshold was 16 μJ (Figs. 10 and 13), which resulted in d_{eff} of 3.6 pm/V. As seen in the 792.5 nm signal energy vs pump energy graph, after the annealing, the BWOPO threshold increased four times (60 μJ), and by using (2) formula, a twofold lower d_{eff} (1.8 pm/V) was estimated. Maximum signal energy and slope efficiency were also ~4 times lower.

The significant reduction in d_{eff} observed after annealing the Rb:PPKTP crystal to 350 °C is attributed to the thermal instability of the ferroelectric domain structure. During the annealing process, redistribution of bulk charges and/or the reorientation of defect dipoles may generate internal fields capable of moving domain walls.[40] The periodic poling homogeneity measurement (Fig. 8) revealed that the ferroelectric domains did not fully propagate through the crystal's entire thickness, resulting in charged domain walls arranged in a tail-to-tail configuration.[41] This suggests that the thermal domain instability can be tentatively linked to the unpinning of the domain ends. Most likely, it happens due

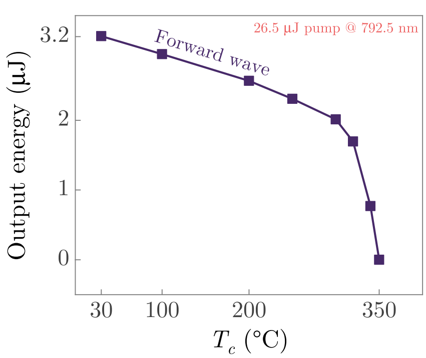

FIG. 12. 792.5 pumped BWOPO forward wave energy decreased with increasing crystal temperature T_c.

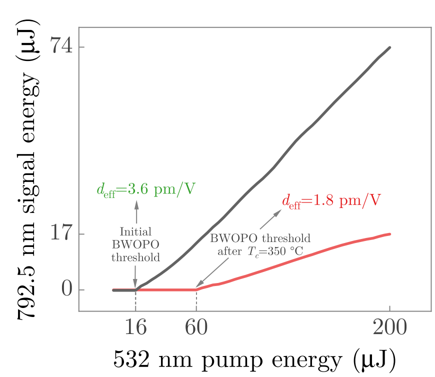

FIG. 13. By measuring the BWOPO oscillation threshold, a twofold reduction in the second-order nonlinear coefficient (d_{eff}) was estimated after annealing the BWOPO crystal to 350 °C.

to domain-stabilizing spatial charge redistribution by thermally activated ionic hopping motion in the K+, K-vacancy system. Therefore, at elevated temperatures, these domains back-switched, reverting to their original polarization orientation prior to poling, which induced changes in the QPM structure. It should be noted that the temperatures used here are well below thermal decomposition temperatures in $KTiOPO_4$.[42,43] In addition, previous experiments showed that the submicrometer grating periods can completely back-switch when annealed at temperatures of 650–730 °C for 4.5 h.[40,41] Here, at 350 °C, complete back-switching did not occur, as the BWOPO remained functional but with significantly reduced efficiency. Since the signal and idler wavelengths remained unchanged after annealing, it is likely that the degradation of the domain duty cycle is primarily responsible for the reduced d_{eff}. Although in the Rb:PPKTP crystal used for high-temperature experiments we observed a decrease of d_{eff} above 320 °C, more investigation is needed to determine how this process is related to the domain pinning and space charge localization in the bulk of the crystal. It could be that the structure with the domains pinned at the surfaces of the crystal will be more resilient to back-switching.

III. CONCLUSION

In this work, we have shown that unique properties of counter-propagating three-wave interactions rendered the BWOPO setup as highly suitable for use in microlaser-based parametric devices, as it allowed us to address the fundamental limitations of conventional OPGs and OPOs relying on co-propagating interactions. We demonstrated the first BWOPO pumped by the transform-limited subnanosecond pulses from a passively Q-switched Nd:YAG microlaser. BWOPO was realized in a periodically poled Rb-doped KTP crystal with one of the shortest QPM grating periods ever produced of 427 nm.

Three BWOPO configurations have been investigated. When pumped with the fundamental harmonic (1064 nm), the BWOPO generated a backward signal wave at 1569.5 nm and a forward idler wave at 3303.5 nm, both of which were inherently narrowband, with spectral bandwidths of 22 and 70 pm, respectively. Compared to microlaser-based OPG and OPO setups, this represents up to three orders of magnitude narrower output bandwidths. Combined with very good spatial coherence of the output, the microlaser-pumped BWOPO achieved features unattainable for conventional OPGs and OPOs—nearly transform-limited pulses and nearly diffraction-limited beams of the signal and idler waves. When pumped with a beam waist diameter of 200 μm, the BWOPO signal wave spectrum remained consistent across the beam profile. However, slight bandwidth broadening due to non-collinear QPM was observed in the case of a larger pump beam (400 μm). The same 427 nm period Rb:PPKTP crystal was also pumped by the microlaser's second harmonic (532 nm), generating a forward signal at 792.5 nm and a backward idler at 1618.5 nm with similar characteristics. The total conversion efficiency in both setups was around 50%. Finally, by pumping the BWOPO crystal at a wavelength of 792.5 nm and tuning the crystal temperature to 320 °C, a degenerate BWOPO operation was reached. A narrowband (around 80 pm at FWHM) counter-propagating signal and idler centered at 1585 nm were obtained. Beyond the degeneracy, unlike in co-propagating parametric devices, the QPM was still achieved and additionally featured a reversal of the wave propagation directions. This experiment revealed a detrimental effect of elevated temperature of submicrometer grating period Rb:PPKTP crystal. Heating the crystal to 350 °C resulted in a twofold decrease in its effective nonlinearity, attributed to the instability of the ferroelectric domain structure due to domain boundary recharging by thermally activated ion hopping.

ACKNOWLEDGMENTS

This research has been carried out in the framework of the "Universities' Excellence Initiative" program by the Ministry of Education, Science, and Sports of the Republic of Lithuania under the agreement with the Research Council of Lithuania (Project No. S-A-UEI-23-6). We would like to acknowledge Mikas Vengris, Rytis Butkus, and Gintaras Tamošauskas (Vilnius University) for their technical support.

AUTHOR DECLARATIONS

Conflict of Interest

The authors have no conflicts to disclose.

Author Contributions

J. Banys: Conceptualization (equal); Data curation (equal); Formal analysis (equal); Investigation (equal); Methodology (equal); Validation (equal); Visualization (equal); Writing – original draft (equal); Writing – review & editing (equal). **J. Jakutis Neto**: Investigation (equal); Software (supporting). **A. Žukauskas**: Conceptualization (equal); Methodology (equal); Resources (equal); Validation (equal). **V. Pašiškevičius**: Conceptualization (equal); Methodology (equal); Resources (equal); Validation (equal); Writing – original draft (equal); Writing – review & editing (equal). **V. Jarutis**: Formal analysis (equal); Supervision (equal); Validation (equal); Writing – review & editing (equal). **J. Vengelis**: Conceptualization (equal); Funding acquisition (equal); Resources (equal); Supervision (equal); Writing – review & editing (equal).

DATA AVAILABILITY

The data that support the findings of this study are available from the corresponding author upon reasonable request.

REFERENCES

[1] J. J. Zayhowski, "Periodically poled lithium niobate optical parametric amplifiers pumped by high-power passively *Q*-switched microchip lasers," Opt. Lett. **22**, 169–171 (1997).

[2] J. Banys, J. Savickytė, O. Balachninaitė, S. Armalytė, V. Tamulienė, V. Jarutis, and J. Vengelis, "Performance investigation of high-efficiency widely tunable subnanosecond optical parametric generator and amplifier based on MgO:PPLN," Opt. Express **30**, 23163–23176 (2022).

[3] W. Wu, X. Li, F. Mei, D. Chen, and R. Yan, "30 mJ, 1 kHz sub-nanosecond burst-mode Nd:YAG laser MOPA system," Opt. Express **27**, 36129–36136 (2019).

[4] H. Qiao, K. Zhong, F. Li, X. Zhang, Y. Zheng, S. Wang, T. Gegen, X. Li, D. Xu, and J. Yao, "Near-diffraction-limit 1-kHz sub-nanosecond diode-end-pumped Nd:YAG laser amplifier via self-compensating spherical aberration," Opt Laser. Technol. **164**, 109486 (2023).

[5]G. Stanionytė, E. Vėjalytė, V. Tamulienė, V. Jarutis, and J. Vengelis, "Subnanosecond widely-tunable in the visible spectrum range LBO based optical parametric amplifier," J. Opt. **24**, 045506 (2022).
[6]G. Stanionytė, V. Tamulienė, R. Grigonis, and J. Vengelis, "Investigation of a widely-tunable subnanosecond BBO-based optical parametric amplifier," Lith. J. Phys. **62**, 10–20 (2022).
[7]B. Lang, S. Mosquera-Vázquez, D. Lovy, P. Sherin, V. Markovic, and E. Vauthey, "Broadband ultraviolet-visible transient absorption spectroscopy in the nanosecond to microsecond time domain with sub-nanosecond time resolution," Rev. Sci. Instrum. **84**, 073107 (2013).
[8]S. Romppanen, H. Häkkänen, J. Kekkonen, J. Nissinen, I. Nissinen, J. Kostamovaara, and S. Kaski, "Time-gated Raman and laser-induced breakdown spectroscopy in mapping of eudialyte and catapleiite," J. Raman Spectrosc. **51**, 1462–1469 (2020).
[9]L. Illés, M. Sági-Kazár, F. Steinbach, R. Hembrom, G. Mihailova, K. Georgieva, K. Solymosi, A. Barócsi, Á. Solti, and S. Lenk, "Fluorescence lifetime of plant leaves with sub-nanosecond resolution," Meas. Sci. Technol. **35**, 085206 (2024).
[10]P. Geiser, U. Willer, D. Walter, and W. Schade, "A subnanosecond pulsed laser-source for mid-infrared lidar," Appl. Phys. B **83**, 175–179 (2006).
[11]M. Carrillo-Fuentes, R. S. Cudney, S. H. Lee, and O. P. Kwon, "Sub-nanosecond terahertz radiation obtained with an aperiodically poled lithium niobate and organic HMQ-TMS," Opt. Express **28**, 24444–24451 (2020).
[12]B. Dolasinski, P. E. Powers, J. W. Haus, and A. Cooney, "Tunable narrow band difference frequency THz wave generation in DAST via dual seed PPLN OPG," Opt. Express **23**, 3669–3680 (2015).
[13]J. Vengelis, V. Jarutis, and V. Sirutkaitis, "Visible supercontinuum generation in photonic crystal fiber using various harmonics of subnanosecond Q-switched laser," Opt. Eng. **55**, 096107 (2016).
[14]J. Banys, S. Armalytė, J. Pimpė, O. Balachninaitė, V. Jarutis, and J. Vengelis, "Enhancing conversion efficiency of MgO:PPLN and Rb:PPKTP crystal-based subnanosecond optical parametric generators by utilizing a supercontinuum seed," Infrared Phys. Technol. **137**, 105158 (2024).
[15]H. Qiao, K. Zhong, F. Li, X. Zhang, S. Wang, Y. Zheng, D. Xu, Q. Sheng, W. Shi, and J. Yao, "Efficient MW-peak-power kHz-repetition-rate sub-nanosecond optical parametric generator tunable from near- to mid-infrared," Opt Laser. Technol. **151**, 108010 (2022).
[16]G. Marchev, P. Dallocchio, F. Pirzio, A. Agnesi, G. Reali, V. Petrov, A. Tyazhev, V. Pasiskevicius, N. Thilmann, and F. Laurell, "Sub-nanosecond, 1–10 kHz, low-threshold, non-critical OPOs based on periodically poled KTP crystal pumped at 1,064 nm," Appl. Phys. B **109**, 211–214 (2012).
[17]B. Bruneteau, B. Faure, J. Debray, G. Souhaité, P. Segonds, H. Ishizuki, T. Taira, and B. Boulanger, "Widely tunable near-infrared optical parametric oscillator based on a 5% MgO:PPLN partial cylinder pumped at 1064 nm by a 1-kHz sub-nanosecond microchip laser," Opt. Lett. **48**, 3669–3672 (2023).
[18]L. Liu, H. Y. Wang, Y. Ning, C. Shen, L. Si, Y. Yang, Q. L. Bao, and G. Ren, "Sub-nanosecond periodically poled lithium niobate optical parametric generator and amplifier pumped by an actively Q-switched diode-pumped Nd:YAG microlaser," Laser Phys. **27**, 055403 (2017).
[19]K. Zhong, H. Qiao, F. Li, X. Zhang, Y. Zheng, S. Wang, D. Xu, and J. Yao, "Tunable narrow-linewidth high-peak-power sub-nanosecond optical parametric generator by injection seeding," Opt. Express **30**, 16479–16488 (2022).
[20]J. Banys, S. Armalytė, J. Pimpė, O. Balachninaitė, V. Jarutis, and J. Vengelis, "Subnanosecond microlaser pumped fan-out grating design MgO:PPLN optical parametric generator continuously tunable from near-to mid-infrared," Opt. Laser Technol. **171**, 110433 (2024).
[21]S. E. Harris, "Proposed backward wave oscillation in the infrared," Appl. Phys. Lett. **9**, 114–116 (1966).
[22]C. Canalias and V. Pasiskevicius, "Mirrorless optical parametric oscillator," Nat. Photonics **1**, 459–462 (2007).
[23]C. Liljestrand, A. Zukauskas, V. Pasiskevicius, and C. Canalias, "Highly efficient mirrorless optical parametric oscillator pumped by nanosecond pulses," Opt. Lett. **42**, 2435–2438 (2017).
[24]C. E. Minor and R. S. Cudney, "Mirrorless optical parametric oscillation in bulk PPLN and PPLT: A feasibility study," Appl. Phys. B **123**, 38 (2017).
[25]A.-L. Viotti, F. Laurell, A. Zukauskas, C. Canalias, and V. Pasiskevicius, "Coherent phase transfer and pulse compression at 1.4 μm in a backward-wave OPO," Opt. Lett. **44**, 3066–3069 (2019).
[26]A. Godard, M. Guionie, J.-B. Dherbecourt, J.-M. Melkonian, and M. Raybaut, "Backward optical parametric oscillator threshold and linewidth studies," J. Opt. Soc. Am. B **39**, 408–420 (2022).
[27]A. Zukauskas, A.-L. Viotti, C. Liljestrand, V. Pasiskevicius, and C. Canalias, "Cascaded counter-propagating nonlinear interactions in highly-efficient sub-μm periodically poled crystals," Sci. Rep. **7**, 8037 (2017).
[28]A. Vågberg, M. Brunzell, M. Widarsson, P. Mutter, A. Zukauskas, F. Laurell, and V. Pasiskevicius, "2.7 μm backward wave optical parametric oscillator source for CO_2 spectroscopy," Opt. Lett. **49**, 4553–4556 (2024).
[29]G. Ehret, C. Kiemle, M. Wirth, A. Amediek, A. Fix, and S. Houweling, "Space-borne remote sensing of CO_2, CH_4, and N_2O by integrated path differential absorption lidar: A sensitivity analysis," Appl. Phys. B **90**, 593–608 (2008).
[30]C. Liljestrand, F. Laurell, and C. Canalias, "Periodic poling of Rb-doped $KTiOPO_4$ by coercive field engineering," Opt. Express **24**, 14682–14689 (2016).
[31]P. Mutter, A. Zukauskas, and C. Canalias, "Domain dynamics in coercive-field engineered sub-μm periodically poled Rb-doped $KTiOPO_4$," Opt. Mater. Express **12**, 4332–4340 (2022).
[32]K. M. Mølster, J. R. Negri, A. Zukauskas, C. S. J. Lee, F. Laurell, and V. Pasiskevicius, "Multi-transversal mode pumping of narrow-bandwidth backward wave optical parametric oscillator," Opt. Express **31**, 24320–24327 (2023).
[33]K. M. Mølster, M. Guionie, P. Mutter, A. Zheng, J.-B. Dherbecourt, J.-M. Melkonian, X. Délen, A. Zukauskas, F. Laurell, P. Georges *et al.*, "Highly efficient, high average power, narrowband, pump-tunable BWOPO," Opt. Lett. **48**, 6484–6487 (2023).
[34]P. Mutter, A. Zukauskas, A.-L. Viotti, C. Canalias, and V. Pasiskevicius, "Phase-locked degenerate backward wave optical parametric oscillator," APL Photonics **8**, 026104 (2023).
[35]M. Katz, D. Eger, M. B. Oron, and A. Hardy, "Erratum: 'Refractive dispersion curve measurement of $KTiOPO_4$ using periodically segmented waveguides and periodically poled crystals' [J. Appl. Phys. 90, 53 (2001)]," J. Appl. Phys. **92**, 7702 (2002).
[36]S. Emanueli and A. Arie, "Temperature-dependent dispersion equations for $KTiOPO_4$ and $KTiOAsO_4$," Appl. Opt. **42**, 6661–6665 (2003).
[37]F. Pignatiello, M. De Rosa, P. Ferraro, S. Grilli, P. De Natale, A. Arie, and S. De Nicola, "Measurement of the thermal expansion coefficients of ferroelectric crystals by a moiré interferometer," Opt. Commun. **277**, 14–18 (2007).
[38]G. Strömqvist, V. Pasiskevicius, and C. Canalias, "Self-established noncollinear oscillation and angular tuning in a quasi-phase-matched mirrorless optical parametric oscillator," Appl. Phys. Lett. **98**, 051108 (2011).
[39]J. Banys, J. Pimpė, O. Balachninaitė, V. Jarutis, and J. Vengelis, "Non-destructive periodic poling quality evaluation of MgO:PPLN and Rb:PPKTP crystals based on crystal translation and parametric light generation," Optik **277**, 170686 (2023).
[40]G. Lindgren, A. Peña, A. Zukauskas, C. Liljestrand, B. Ménaert, B. Boulanger, and C. Canalias, "Thermal stability of ferroelectric domain gratings in Rb-doped KTP," Appl. Phys. Lett. **107**, 082906 (2015).
[41]H. Kianirad, G. Lindgren, A. Peña, A. Zukauskas, B. Ménaert, F. Laurell, B. Boulanger, and C. Canalias, "Stabilization of domain structures in Rb-doped $KTiOPO_4$ for high-temperature processes," Appl. Phys. Lett. **114**, 052904 (2019).
[42]J. C. Jacco, G. M. Loiacono, M. Jaso, G. Mizell, and B. Greenberg, "Flux growth and properties of $KTiOPO_4$," J. Cryst. Growth **70**, 484–488 (1984).
[43]M. E. Hagerman, V. L. Kozhevnikov, and K. R. Poeppelmeier, "High-temperature decomposition of potassium titanyl phosphate, $KTiOPO_4$," Chem. Mater. **5**, 1211–1215 (1993).